Li-Ion Battery State of Health Estimation and Remaining Useful Life Prediction Through a Model-Data-Fusion Method

Zhiqiang Lyu, Renjing Gao, and Lin Chen

***Abstract*—The prognostics and health management of Li-ion batteries in electric vehicles are challenging due to the time-varying and nonlinear battery degradation. This article proposes a model-data-fusion method for battery state-of-health estimation and remaining useful life prediction. First, combined with metabolic gray model and multiple-output Gaussian process regression, a dynamic and data-driven battery degradation model is established to simulate battery complicated degradation behaviors, which takes the capacity degradation as the state variable and takes the internal resistance and polarization resistance from battery Thevenin model as the input variables. Second, to suppress the measurement noises of online battery information, a particle filter is utilized to track the battery capacity degradation for state-of-health estimation and extrapolate the degradation trajectory for remaining useful life prediction. Furthermore, battery ageing experiments are conducted to verify the proposed model-data-fusion method. The verification results show that the proposed method can provide an accurate and robustness state of health estimation and remaining useful life prediction at different temperatures.**

***Index Terms*—Li-ion battery, metabolic gray model, model-data-fusion, multiple-output Gaussian process regression, particle filter (PF), remaining useful life, state of health.**

I. Introduction

DEVELOPING with the national energy-saving and emissions-reducing, electric vehicle (EV) has gained great momentum in recent years from governments, industries, and customers. Due to the high power/energy density, long service life, and low environmental pollution [1], Li-ion Battery (LIB) has been widely applied as the power supply for EVs. Among the subjects in the operation of LIBs, battery state-of-health (SOH) estimation and remaining useful life (RUL) prediction are significant, because electrical properties, security, and stability alterations would reduce with an ongoing battery degradation [2]. Battery SOH is defined as a percentage that reflects internal resistance increase or capacity decrease. In EVs, the commonest and most extensive threshold of SOH is that battery maximum available capacity reduces to its 70–80% of the initial capacity. Another threshold based on internal resistance is when battery resistance reaches 160% or 200% of the initial resistance under conditions of the same state-of-charge (SOC) and operating temperature. While RUL is defined as the charge–discharge cycles or time span from the current time to the life threshold [3]. Accurate SOH estimation and RUL prediction of LIBs can provide predictive maintenance and replacement of the battery power system in EVs [4], [5]. To accurately monitor the degradation behaviors of LIBs, a battery management system (BMS) with specific embedded processes and methods is indispensable. Over recent years, extensive methods research on the SOH estimation and RUL prediction have been conducted.

A. Review of the Methods for SOH

For battery SOH estimation, according to the method characteristics, these methods can be mainly divided into three classes: experimental methods, model-based methods, and data-driven methods [5].

1) *Experimental Methods:* As the name implies, the experimental methods analyze the battery ageing behaviors with extensive experiments. One of the experimental methods is Coulomb counting method, the LIB was fully charged, then, discharged at a low discharge rate, and the discharged electricity was counted to determine battery SOH. Another frequently used technique, impedance measurement, was utilized to calculate SOH through the correlation between SOH and impedance. Ohm's law and Electrochemical Impedance Spectrum (EIS) were primary tools. Besides, incremental capacity analysis [6] and differential voltage analysis [7] were utilized to analyze capacity degradation. Limited by the discharge rate or specialized experimental equipment, experimental methods have limited application scenarios, e.g., laboratory environments [8].

Manuscript received May 26, 2020; revised July 28, 2020; accepted October 20, 2020. Date of publication October 23, 2020; date of current version February 5, 2021. This work was supported in part by the National Natural Science Foundation of China under Grants 11572073 and U1808215, and in part by the 111 Project (B14013) and the Fundamental Research Funds for the Central Universities (DUT18ZD103). Recommended for publication by Associate Editor C. N. M. Ho. *(Corresponding author: Renjing Gao.)*

Zhiqiang Lyu and Renjing Gao are with the State Key Laboratory of Structural Analysis for Industrial Equipment, Dalian University of Technology, Dailian 116024, China and also with the Ningbo Institute of Dalian University of Technology, Ningbo 315016, China (e-mail: bushlv@hotmail.com; renjing@dlut.edu.cn).

Lin Chen is with the Guangxi University, Nanning 542400, China (e-mail: gxdxcl@163.com).

This article has supplementary downloadable material available at https://ieeexplore.ieee.org, provided by the authors.

Color versions of one or more of the figures in this article are available online at https://ieeexplore.ieee.org.

Digital Object Identifier 10.1109/TPEL.2020.3033297

2) *Model-Based Methods:* To realize online and reliable monitoring of battery degradation, model-based methods are introduced. The model-based methods combined electrochemical model or equivalent circuit model (ECM) with adaptive filters involving the closed-loop and feedback control [9]. The electrochemical model describes the electrochemical reactions inside LIBs using some differential equations, offers insights and knowledge about battery degradation mechanisms, thus, has high estimation accuracy [10]. Due to the heavy computation cost of the solution procedure, the simplification of the electrochemical model gains great attention. For instance, Zheng *et al.* [11] presented a numerical solution for an electrochemical model, the iteration-approaching method was incorporated with the trinal proportional-integral observers to enhance the estimation performance of SOC, capacity, and resistance in energy storage system (EES). With a reduced-order electrochemical model, Lin *et al.* [12] used two separate sliding mode observers for joint SOC and SOH estimation and verified the estimation performance using the LiFePO4/graphite battery in EVs. For EV and grid storage, Lyu *et al.* [13] proposed an activation-and-response analysis method to identify the parameters of a simplified single-particle model, and the model parameters were proved to have strong correlations with battery capacity degradation. Considering the chemical/mechanical degradation physics, Li *et al.* [14] developed an advanced single-particle-based degradation model, and the model provided quantitative information regarding solid electrolyte interface formation and cracks propagation for the SOH estimation in EVs. However, the calculative burden for electrochemical model still hinders its possibility in BMS. Alternatively, ECM is developed by circuit elements to depict static and dynamic characteristics while neglecting battery physicochemical ageing mechanisms. By taking SOC and capacity as state variables, a multitime scale extended Kalman filter (EKF) was used for combined SOC/SOH monitoring based on the Thevenin model [15]. Afshari *et al*. [16] proposed a smooth variable structure filter for battery SOH estimation in EES using the chattering signal and without the need for modeling the batteries, the proposed smooth variable structure filter can provide more accurate estimation accuracy of SOC and SOH than EKF. To avoid the linearization of EKF, based on the real-time current and voltage, Schwunk *et al.* [17] proposed a particle filter (PF) to achieve SOC and SOH estimation of LiFePO4/graphite battery using the same estimation framework. Considering the variation of resistance with SOC, Shi *et al.* [18] proposed an improved unscented PF to track the resistance based on a second-order resistor–capacitor model in EVs, then, SOH was calculated through the resistance-based definition. Taken as a whole, the model-based methods estimate the model ageing parameters which are sensitive to battery degradation and have high application potential. However, a common and accurate ageing model is necessary for these methods.

3) *Data-Driven Methods:* The data-driven methods describe battery internal degradation evolution through the abundant pretest data and some machine learning algorithms without expert knowledge on ageing mechanisms. For instance, Piao *et al*. [19] proposed a hidden Markov model to analyze battery health status in EVs based on the stochastic relationship between resistance and lifetime. You *et al.* [20] designed a long short-term memory to improve the performance of the recurrent neural network, then, the measurable battery data in EVs were used to estimate battery SOH with the average error lower than 2.46%. For EES, Meng *et al.* [21] captured the relationship between the features from the terminal voltage response of LIBs under current pulse test and SOH using the support vector regression (SVR). Guo *et al.* [22] extracted the health features from the charging stage of EV, and the relevance vector machine (RVM) was used to calculate SOH with the optimized health features by principal component analysis. These types of methods are flexible, however, have high requirements on the effectiveness and portability of the machine learning algorithms. Besides, relative to model-based methods, data-driven methods are an open-loop estimation framework essentially, thus, highly depend on the transmitted data.

B. Review of the Methods for RUL

For the RUL prediction, it needs to judge the future battery degradation trend instead of direct measurement. The prediction techniques include model-based methods, data-driven methods [4], [23].

1) *Model-Based Methods:* There are few articles which present battery ageing models to predict RUL, the combination of empirical models and adaptive filters are mainstream battery degradation models. For instance, Liu *et al.* [24] proposed a capacity degradation model considering the cycling current in the hybrid EES, and PF was used for the long-term RUL prediction. Based on the double-exponential capacity degradation model [25], Zhang *et al.* [26] addressed the problem of the sample degeneracy phenomenon in unscented particle filter (UPF) using the Markov chain Monte Carlo for hybrid EVs. The improved UPF demonstrated the effectiveness of the RUL prediction. Walker *et al.* [27] contrasted the nonlinear least squares, PF, and Unscented Kalman Filter (UKF) for the RUL prediction with three separate models of LIBs. Besides, for the electronic systems, Duong *et al.* [28] introduced a heuristic Kalman algorithm to tackle sample degeneracy and impoverishment of standard PF. The Heuristic PF performed better on the RUL prediction than PF, UPF, and particle swarm optimized PF. The model-based RUL prediction methods can improve the accuracy of health prognostic. However, the model accuracy is easily influenced by external and internal factors [5], such as SOC and loading profiles, then, the RUL prediction accuracy is affected.

2) *Data-Driven Methods:* For the satellite batteries, Saha *et al.* [29] developed a lumped parameter model based on the EIS test and constructed an ageing model based on RVM and offline EIS. Combined with exponential curve fitting, quadratic functions, SVR, and EIS test, Wei *et al.* [3] constructed an SVR-based capacity degradation model, and PF was employed to estimate degradation parameters for the SOH estimation and RUL prediction. To avoid the offline EIS test, Zhou *et al.* [30] proposed the mean voltage falloff in the constant-current discharging period for battery degradation modeling, and an optimized RVM was employed to predict the battery RUL in EVs. Parthiban *et al.* [31] designed an artificial neural network to approximate the relation between the charge–discharge cycle and battery capacity, the short-term predictive capability performed better than the long-term prediction. To enhance the prediction performance, Liu *et al.* [32] proposed an incremental optimized RVM algorithm with a flexible training strategy, the proposed method had a low computational burden and excellent RUL prediction performance. Khumprom *et al.* [33] presented deep neural networks to predict SOH and RUL of LIBs, moreover, the proposed deep neural network was compared against other machine learning algorithms. Li *et al.* [34] proposed a hybrid model to predict the battery RUL in EVs by combining the long short-term memory and Elman neural networks to predict high- and low-frequency sublayers, respectively. Inevitably, individual training data points have an even greater impact on predicting accuracy for these methods. Besides, the immeasurable battery capacity is also another obstacle to obtain the training dataset for the RUL prediction.

C. Contribution of the Article

In the light of these previous works, whether SOH estimation or RUL prediction, accurate battery degradation models are necessary. The parameters in the degradation models should be estimated through an online process, so real-time battery health status can be monitored. When RUL is predicted, no online and future battery information can be measured, the historical battery parameters should be employed to predict the capacity degradation trend. Moreover, interval estimation is also essential to express the uncertainty of RUL prediction.

In this article, a model-data-fusion method is developed for battery SOH estimation and RUL prediction. Based on battery Thevenin model, ohmic resistance and polarization resistance are as the representative ageing features to quantify battery capacity degradation. Further, considering the coupling relationship between the two ageing features, then, combined battery temperature, metabolic gray model (MGM), and multioutput Gaussian process regression (MOGPR), a dynamic and data-driven state-space representation for battery ageing modeling is constructed. Finally, to suppress the system noise, PF is further used to track the battery capacity degradation for the SOH estimation. Meanwhile, the output of PF is employed to update the state-space representation for closed-loop control and dynamic model updating. Based on the SOH estimation results, RUL prediction with probability distribution is achieved.

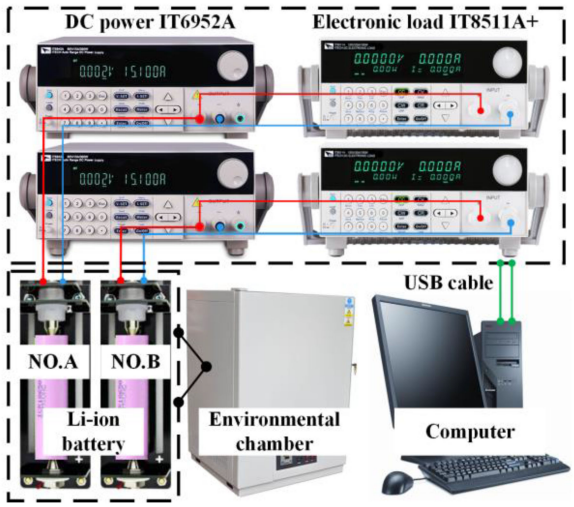

Fig. 1. Extensible multichannel battery testing system [36], [37].

D. Organization of the Article

The rest of this article is organized as follows. Section II introduces the definitions of SOH and RUL, then, battery ageing test is introduced. Section III introduces the battery Thevenin model and ageing features for battery degradation modeling. Section IV describes the PF, MGM, MOGPR, and the proposed model-data-fusion method for SOH estimation and RUL prediction in detail. Section V provides simulation results and verification. Finally, Section VI concludes this article.

II. Li-Ion Battery Ageing Test

In this article, the capacity-based definitions of SOH and RUL are adopted

$$\begin{cases} SOH_i = \frac{C_i}{C_1} \times 100\% \\ RUL_i = |Cycle_i - Cycle_{\text{total}}| \end{cases} \tag{1}$$

where SOH_i, C_i are the values of SOH and battery capacity in the ith test, respectively, while C_1 is the initial battery capacity at a certain temperature. RUL_i is the predicted RUL (or cycles(after i accumulated cycles ($Cycle_i$), and $Cycle_{\text{total}}$ is the total cycles that battery goes through from a fresh battery to the life threshold. Over the lifetime of LIBs, battery capacity gradually decreases due to the irreversible physical and chemical reactions. When the SOH drops below 80%, the batteries may be no longer usable in EVs [2], [9].

To simulate the complex working environment of the batteries in EV, a series of dynamic charging and discharging cycles are carried out at different temperatures with an extensible multichannel battery testing system [35], [36], as shown in Fig. 1. The experimental procedure for accelerated degradation of batteries is shown in Table I.

As shown in Fig. 1, the batteries manufactured by Samsung, labeled ICR18650-26F, numbered A and B, are tested [36], [37].

TABLE I
AGEING EXPERIMENTAL PROCEDURE OF BATTERIES

Step 1: Characteristic test, including capacity test, New European Driving Cycle (NEDC) test, Urban Dynamometer Driving Schedule (UDDS) test, and Japanese 10-15 mode driving cycle (JP1015) test at 10 °C.
Step 2: Characteristic test, including capacity test, NEDC test, UDDS test, and JP1015 test at 25°C.
Step 3: Characteristic test, including capacity test, NEDC test, UDDS test, and JP1015 test at 40°C.
Step 4: Composite loading for 3 times at 45 °C for the accelerated ageing test.
Step 5: Return to **Step 1** until the maximum capacity is less than 80% of the nominal capacity at 25°C.

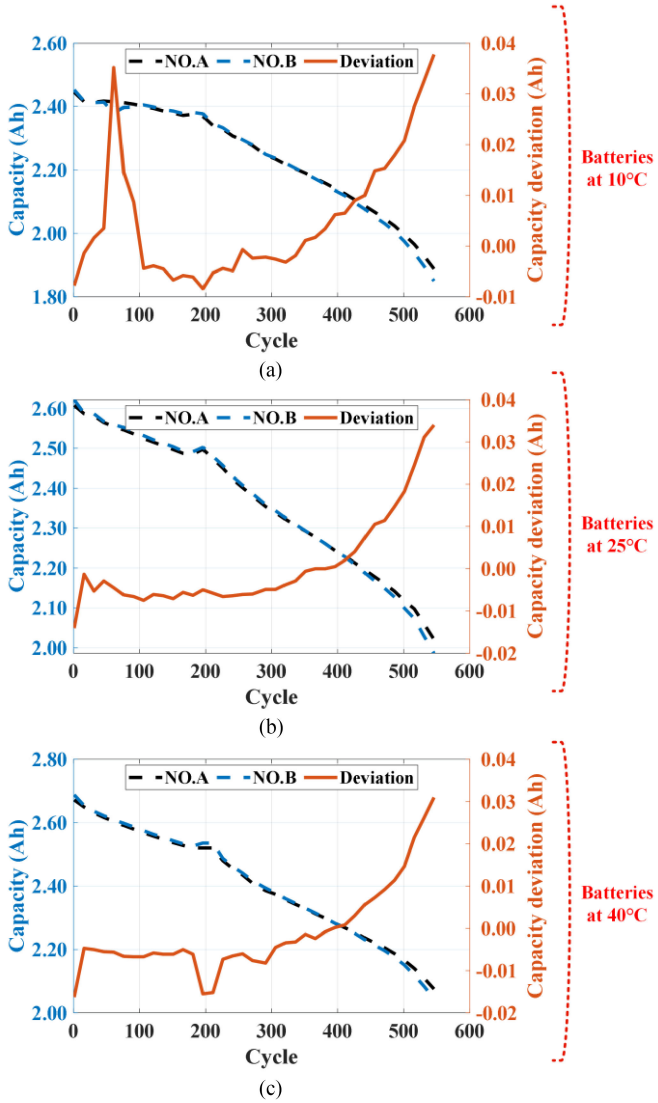

Fig. 2. Capacity and capacity deviation.

The materials consist of graphite on the anode and LiNMC on the cathode. According to the experimental procedure (see Table I), the evolution of the capacities of two batteries over the degradation process at different temperatures is shown in Fig. 2.

As shown in Fig. 2, battery capacity tends to nonlinearly decrease when the cycle increases. Although the two batteries are tested in the same environment, the capacities still show some differences due to the inconsistency caused by ageing, and the differences increase gradually with the ageing cycle.

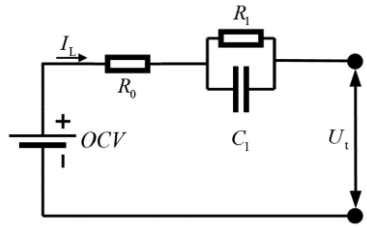

Fig. 3. Battery Thevenin model.

III. BATTERY MODEL AND AGEING FEATURES

ECMs, as the lumped models with relatively few numbers of parameters, have been studied to depict static and dynamic characteristics of LIBs. Hu *et al.* [38] compared 12 commonly used ECMs and considered the Thevenin model to be preferred for LiNMC batteries. Xiong *et al.* [9], [10] pointed out that the Thevenin model is more suitable for on-board use in BMS to simulate the battery performance based on the balance between model accuracy and complexity. Herein, the Thevenin model is employed for battery modeling. Thevenin model contains an open-circuit voltage, ohmic resistance (R_0), and a resistor–capacitor ($R_1//C_1$) network, as shown in Fig. 3.

For the batteries in EVs, the terminal voltage $U_{\rm t}$, loading current $I_{\rm L}$, and temperatures are easy to measure directly. Based on these direct measured battery information and recursive least-squares method [9], [15], the model parameters are identified in real time. According to [39], [40], battery identified resistances (R_0, R_1) keep a constant basically in the intermediate region of SOC.

The power battery system consists of hundreds of batteries connected in series and parallel [5]. However, LIBs with different attended modes (such as wire diameters and welding manners) may lead to different measured internal resistance. Besides, the inconsistency and the external resistance between batteries also leads to different battery maximum available capacity. To eliminate the effects of connection types and inconsistency on initial resistance and capacity, in [35], we have defined the increment of internal ohmic resistance (ΔR_0) and polarization resistance (ΔR_1) of the Thevenin model as the ageing features to quantify battery capacity degradation (ΔC)

$$\begin{cases} R_0^i = \frac{1}{n}\left(R_0(SOC=30\%) + \cdots R_0(SOC=80\%)\right) \\ R_1^i = \frac{1}{n}\left(R_1(SOC=30\%) + \cdots R_1(SOC=80\%)\right) \\ \Delta R_0^i = \left|R_0^i - R_0^1\right| \\ \Delta R_1^i = \left|R_1^i - R_1^1\right| \\ \Delta C_i = \left|C_1 - C_i\right|. \end{cases} \tag{2}$$

Pearson correlation analysis, the most extensively used method to measure correlation as shown in (3), is employed to quantitatively evaluate the correlation between two features and capacity degradation. Besides, a 95% confidence interval

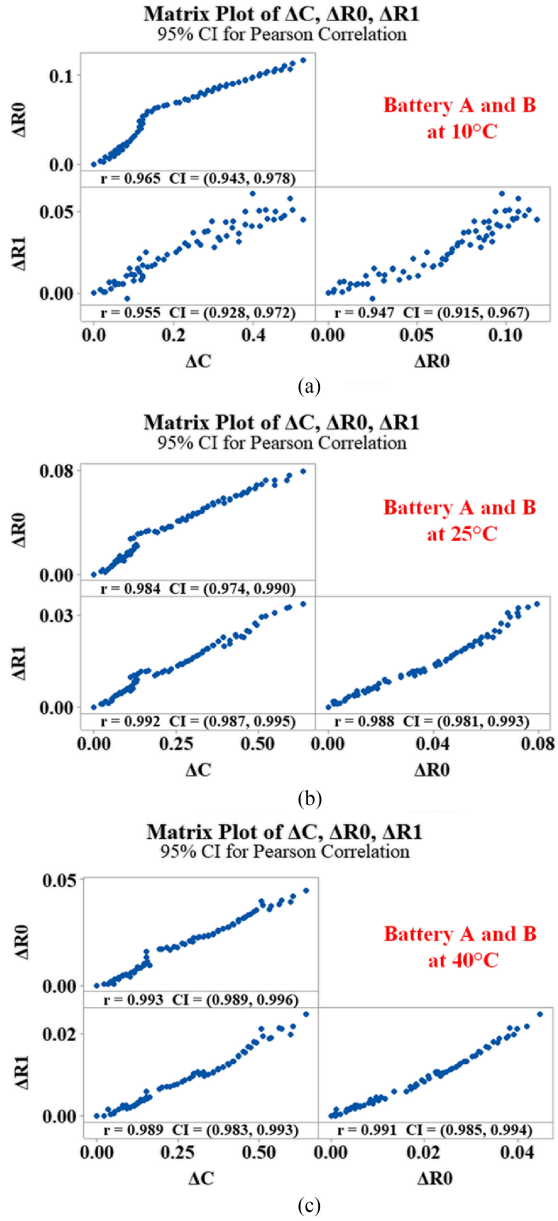

Fig. 4. Correlation analysis.

for the Pearson correlation is illustrated in Fig. 4

$$r = \frac{\sum (X - \bar{X})(Y - \bar{Y})}{\sqrt{\sum (X - \bar{X})^2}\sqrt{(Y - \bar{Y})^2}} \tag{3}$$

where $\bar{X}$ is the mean of X sequence and $\bar{Y}$ is the mean of Y sequence.

As shown in Fig. 4, at 10 °C, the Pearson correlation coefficients between the ageing features and capacity degradation are minimal, about 0.95. At higher temperatures, the Pearson correlation coefficients significantly increase to about 0.98. Generally, a Pearson correlation coefficient of ± 0.8 indicates a strong correlation between the two variables. Thus, the capacity degradation exhibits a high correlation with the two ageing features according to the calculated Pearson coefficients and the 95% confidence intervals (CIs). In addition, the correlation coefficients between the ageing features are greater than 0.94 at various temperatures. The result suggests that there is also a strong coupling relationship between the two ageing features.

However, the estimation framework in [35] is open-loop. Herein, the same ageing features are employed to develop a dynamic, close-loop, and model-data-fusion method for the SOH estimation and RUL prediction.

IV. Methods

The primary missions of this article are to develop a dynamic and data-driven state-space representation to describe battery degradation, then develop a model-data-fusion method for the battery SOH estimation and RUL prediction. In this case, the MGM-based and MOGPR-based capacity degradation models are employed to construct a dynamic battery ageing model, while PF is utilized to track or extrapolate capacity degradation according to the ageing features in every dynamic test.

A. Particle Filter

Sankararaman *et al.* [41] pointed out that the Bayesian interpretation of uncertainty is more suitable for the RUL prediction in the context of condition-based monitoring. PF is a sequential Monte Carlo method for online learning within the Bayesian framework, which has been reviewed in [42]. PF focuses on a general situation for the nonlinear state-space model with non-Gaussian noise assumption, while the KF family, such as EKF or UKF, is based on a local linearized state-space model with Gaussian noise assumption. The basic idea of PF is that the posterior density is represented by a set of random particles with associated weights. Thus, PF has the potential to be one of the core algorithms in BMS for the battery SOH estimation and RUL prediction.

For a nonlinear and dynamic system, a state-space representation is a general mathematical model to describe the relationship among a set of the measurable observation (z) and unknown state variable (x)

$$\begin{cases} x_k = f\left(x_{k-1}, w_{k-1}\right) \Leftrightarrow (a) \\ z_k = h\left(x_k, v_k\right) \Leftrightarrow (b) \end{cases} \tag{4}$$

where $f(\bullet)$ and $h(\bullet)$ are the nonlinear functions to be estimated,w and v are non-Gaussian noise, respectively.

Based on the state-space representation, the state estimation of the dynamic system can be performed according to the procedures of PF shown in Table II.

B. State-Space Representation

In the state-space representation shown in (4), state equation describes the time recursion between two adjacent state variables, while the observation equation describes the relationship between the observations and the unknown state variable. For the SOH estimation and RUL prediction of LIBs, a dynamic and general state-space representation is critical to improve the estimation and prediction accuracy.

TABLE II
PARTICLE FILTER STEP 1: INITIALIZATION: GENERATE A SAMPLE SET

Step 1: Initialization: Generate a sample set $\left\{\mathbf{x}_0^i\right\}_{i=1}^N$ from the initial distribution $p(\mathbf{x}_0)$, set $k=1$.
Step 2: Time update: based on Eq.(4) a, draw the predicted sample $x_k^i \sim p\left(x_k \mid x_{k-1}^i\right), i=1,2,\cdots,\boldsymbol{N}$.
Step 3: Observation update: once the observation z_k is measured, evaluate the weight of the sample $\tilde{w}_k^i = w_{k-1}^i p\left(z_k \mid x_k^i\right)$, and normalize $w_k^i = \tilde{w}_k^i \Big/ \sum_{q=1}^N \tilde{w}_k^q, i=1,2,\cdots,\boldsymbol{N}$ based on Eq. (4) b.
Step 4: Resampling: generate a new sample set $\left\{x_k^j\right\}_{j=1}^N$ by resampling (with replacement) N times from $\left\{x_k^i\right\}_{i=1}^N$, where, $\Pr\left(x_k^j = x_k^i\right) = w_k^i$, and set weight $w_k^i = 1/N$.
Step 5: Obtain the estimation results $\hat{x}_k = \sum_{j=1}^N w_k^j x_k^j$.
Step 6: set $k=k+1$ and return to **Step 2**.

1) MGM-Based Battery Degradation State Equation: To describe battery capacity degradation, the state variable is taken as battery capacity ΔC. Then, the issue to establish the degradation model is transformed to approximate the relation between historical capacity degradation and next-time capacity degradation ΔC_{k+1}:

$$\Delta C_{k+1} = f\left(\Delta C_m, \Delta C_{m+1}, \cdots, \Delta C_{k-1}, \Delta C_k\right) \tag{5}$$

where $f(\bullet)$ is a function to describe the battery degradation mechanism. Because of the complex electrochemical reactions, it is difficult or even impossible to determine the unknown functional coefficients of $f(\bullet)$ without specific expressions. Herein, Gray Model (GM) is employed to replace $f(\bullet)$. GM (1,1) is currently one of the most widely used gray prediction models [43]. It is a linear dynamic first-order single sequence prediction model for the discrete form of the differential equation for time series prediction, which can be established using at least four data points. The procedure of GM (1,1) is expressed as follows.

Step 1: Establish a non-negative sequence $X^{(0)}$ using the historical capacity degradation data for model initialization:

$$X^{(0)} = \left(\Delta C_1^{(0)}, \Delta C_2^{(0)}, \cdots, \Delta C_k^{(0)}\right) \tag{6}$$

where $\Delta C_k^{(0)} \geq 0,\ k = 1, 2, \cdots n.$

Step 2: Generate the first-order accumulated generating operation sequence $X^{(1)}$ to suppress noise and randomness based on the initial sequence $X^{(0)}$:

$$X^{(1)} = \left(\Delta C_1^{(1)}, \Delta C_2^{(1)}, \cdots, \Delta C_k^{(1)}\right) \tag{7}$$

where $\Delta C_k^{(1)}$ is derived as the following equation:

$$\Delta C_k^{(1)} = \sum_{i=1}^{k} \Delta C_k^{(0)},\ k = 1, 2, \ldots n. \tag{8}$$

Step 3: Define the first-order differential whitening equation of sequence

$$\frac{d\left(\Delta C_k^{(1)}\right)}{dt} + a\left(\Delta C_k^{(1)}\right) = b. \tag{9}$$

Above, $\hat{a} = [a, b]^{\mathrm{T}}$ is a sequence of parameters that can be conducted by

$$\hat{a} = \left(B^{\mathrm{T}} B\right)^{-1} B^{\mathrm{T}} Y \tag{10}$$

where $Y = [\Delta C_2^{(0)}, \Delta C_2^{(0)}, \ldots, \Delta C_2^{(0)}]^{\mathrm{T}}$,

$$B = \begin{bmatrix} -\frac{1}{2} \times \left(\Delta C_2^{(1)} + \Delta C_1^{(1)}\right) & 1 \\ -\frac{1}{2} \times \left(\Delta C_3^{(1)} + \Delta C_2^{(1)}\right) & 1 \\ \vdots & \vdots \\ -\frac{1}{2} \times \left(\Delta C_n^{(1)} + \Delta C_{n-1}^{(1)}\right) & 1 \end{bmatrix}.$$

Step 4: Compute the time response function of $\Delta C_{k+1}^{(1)}$ at time $k+1$ according to (9)

$$\Delta C_{k+1}^{(1)} = \left[\Delta C_1^{(0)} - \frac{b}{a}\right] e^{-ak} + \frac{b}{a}. \tag{11}$$

To obtain the predicted value of the original sequence, the inverse accumulated generating operation is operated

$$\Delta C_{k+1}^{(0)} = \Delta C_{k+1}^{(1)} - \Delta C_k^{(1)} = \left[\Delta C_1^{(0)} - \frac{b}{a}\right] e^{-ak}\left(1 - e^{a}\right). \tag{12}$$

As the LIBs age, the ageing trend may have different characteristics. Meanwhile, the data size of the historical capacity degradation increases, which requires more and more calculation power for prediction. To obtain the latest information for modeling and reduce the calculation power, the metabolism is introduced to construct an MGM and enhance the prediction accuracy. The schematic diagram of MGM is shown in Fig. 5.

As illustrated in Fig. 5, the procedure of MGM can be divided into four steps.

Step 1: The GM (1, 1) is implemented to predict the next-time capacity degradation.
Step 2: The predicted capacity degradation is updated by external information updating.
Step 3: For the sequence reconstruction, the oldest data point of capacity degradation is removed, and the updated capacity degradation is introduced through the metabolism.
Step 4: Return to Step 1 for the next prediction.

Herein, MGM is used to build a dynamic state equation to predict battery capacity degradation trajectory. In other words, the predicted capacity degradation is as the prior information, then, updated by external information to reconstruct the prediction series.

2) MOGPR-Based Battery Degradation Observation Equation: In the previous section, the prior capacity degradation is predicted based on the MGM. The capacity predicted degradation trajectory would deviate from the actual trajectory with never correction. Thus, it is significant to update the predicted prior estimate through the observable ageing features. However,

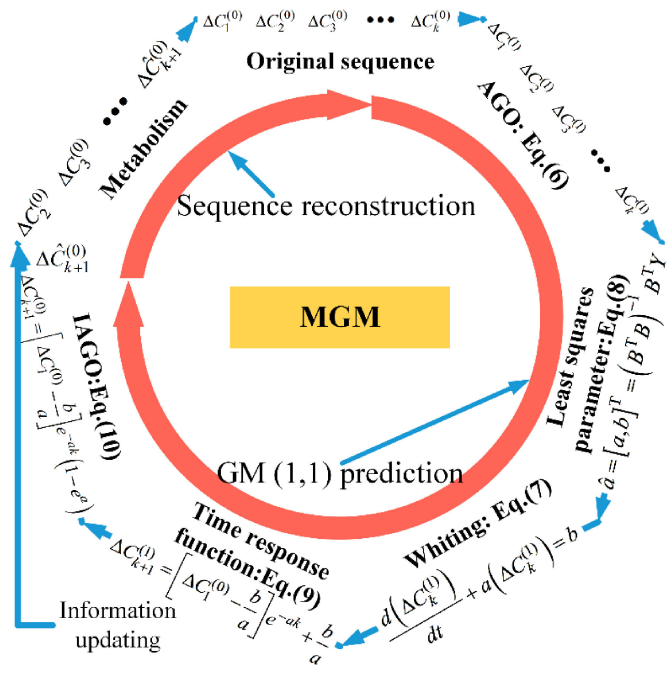

Fig. 5. Metabolic gray model.

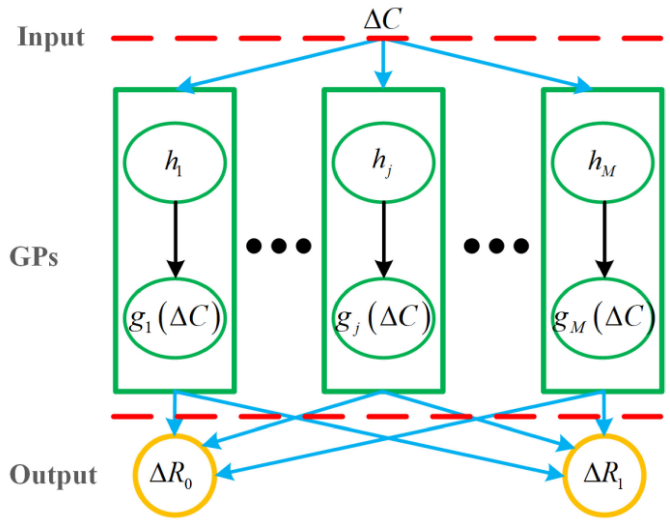

Fig. 6. Multioutput GPR [44].

there exist high relevance and particularity between the two online ageing features (see Fig. 4). Herein, MOGPR is introduced to treat with such a multiple-input-multiple-output problem, and the ageing-features-based degradation model is established to update the MGM-based prediction results (information updating in Fig. 5).

The MOGPR is employed to establish the nonlinear function$h(\bullet)$, then intends to approximate the two outputs $\{\Delta R_0, \Delta R_1\}$ simultaneously using the capacity degradation as the input by considering their correlations, to outperform individual modeling, as shown in Fig. 6.

Like the single-output Gaussian process regression (GPR) [45], [46], the two outputs $\{\Delta R_0, \Delta R_1\}$ are supposed to follow a Gaussian process (GP)

$$\mathbf{f}(\Delta C)\mathcal{GP}\left(\mathbf{0}, \mathcal{K}_M\left(\Delta C, \Delta C'\right)\right). \tag{13}$$

In a GP, the multioutput covariance matrix $\mathcal{K}_M(\Delta C, \Delta C') \in R^{2\times 2}$ can be expressed as

$$\mathcal{K}_M\left(\Delta C, \Delta C'\right) = \begin{bmatrix} k_{11}\left(\Delta C, \Delta C'\right) & k_{12}\left(\Delta C, \Delta C'\right) \\ k_{21}\left(\Delta C, \Delta C'\right) & k_{22}\left(\Delta C, \Delta C'\right) \end{bmatrix}. \tag{14}$$

Every element $k_{tt'}(\Delta C, \Delta C')$ in the covariance matrix corresponds to the covariance, i.e., the degree of correlation or similarity, between outputs ΔR_0 and ΔR_1.

Given the nonlinear relationship:

$$y_t(\Delta C) = f_t(\Delta C) + \epsilon_t \tag{15}$$

where the independent identically distributed Gaussian noise $\epsilon_t \mathcal{N}(0, \sigma_{s,t}^2)$ is assigned to each output, the likelihood function for the T outputs follows:

$$p\left(\mathbf{y}|\mathbf{f}, \Delta C, \Sigma_s\right) = \mathcal{N}\left(\mathbf{f}(\Delta C), \Sigma_s\right) \tag{16}$$

where $\Sigma_s \in R^{T\times T}$ is a diagonal matrix with the elements $\{\sigma_{s,t}^2\}_{1\le t\le T}$.

When the training set $\Delta C = \{\Delta C_1, \ldots, \Delta C_T\}^T$ and output observations $\mathbf{y} = \left\{\begin{Bmatrix}\Delta R_0 \\ \Delta R_1\end{Bmatrix}_1, \ldots, \begin{Bmatrix}\Delta R_0 \\ \Delta R_1\end{Bmatrix}_{1T}\right\}^T$ are employed to training a MOGPR, then, a new test point $\Delta C*$ is inputted to the MOGPR, the predicted posterior distribution $\mathbf{f}(\Delta C_*) = \{f_1(\Delta C_*), \ldots, f_T(\Delta C_*)\}^T$ of the model output is

$$\mathbf{f}\left(\Delta C_*\right)|\Delta C, \mathbf{y}, \Delta C_* \mathcal{N}\left(\widehat{\mathbf{f}}\left(\Delta C_*\right), \Sigma_*\right). \tag{17}$$

Thus, the mean and variance are as follows:

$$\begin{cases} \widehat{\mathbf{f}}\left(\Delta C_*\right) = K_{M*}^{\mathrm{T}}\left[K_M(\Delta\bar{C}, \Delta\bar{C}) + \Sigma_M\right]^{-1}\mathbf{y} \\ \Sigma_* = \mathcal{K}_M\left(\Delta C_*, \Delta C_*\right) \\ \qquad -K_{M*}^{\mathrm{T}}\left[K_M(\Delta\bar{C}, \Delta\bar{C}) + \Sigma_M\right]^{-1}K_{M*} \end{cases} \tag{18}$$

where $K_{M*} = K_M(\bar{X}, \Delta C_*) \in R^{nT\times T}$ has blocks $K_{tt'}(\bar{X}, \Delta C_*) = [k_{tt'}(\Delta C_i, \Delta C_*)]$ for $i = 1, \ldots, n$ and $t, t' = 1, \ldots, T$; $\mathcal{K}_M(\Delta C_*, \Delta C_*) \in R^{T\times T}$ has elements $k_{tt'}(\Delta C_*, \Delta C_*)$ for $t, t' = 1, \ldots, T$; each diagonal element of $\Sigma*$ corresponds to $\sigma_t^2(\Delta C_*)$; and $\Sigma_M = \Sigma_S \otimes I_n \in R^{nT\times nT}$ is a diagonal noise matrix; the symmetric and block partitioned matrix $K_M(\Delta\bar{C}, \Delta\bar{C}) \in R^{nT\times nT}$ is calculated by (14) as

$$K_M(\Delta\bar{C}, \Delta\bar{C}) = \begin{bmatrix} K_{11}(\Delta\bar{C}, \Delta\bar{C}) & \cdots & K_{1T}(\Delta\bar{C}, \Delta\bar{C}) \\ \vdots & \ddots & \vdots \\ K_{T1}(\Delta\bar{C}, \Delta\bar{C}) & \cdots & K_{TT}(\Delta\bar{C}, \Delta\bar{C}) \end{bmatrix}. \tag{19}$$

Covariance matrix represents the covariance of all outputs, so MOGPR can model multiple outputs and capture the correlation between multiple outputs.

Therefore, MOGPR can capture the underlying relationship between the input and outputs, and the coupling relationship between the outputs. Herein, the capacity degradation (ΔC) of the reference battery is as the training/input set, the two ageing features ($\Delta R_0, \Delta R_1$) are as the outputs, as shown in Fig. 6.

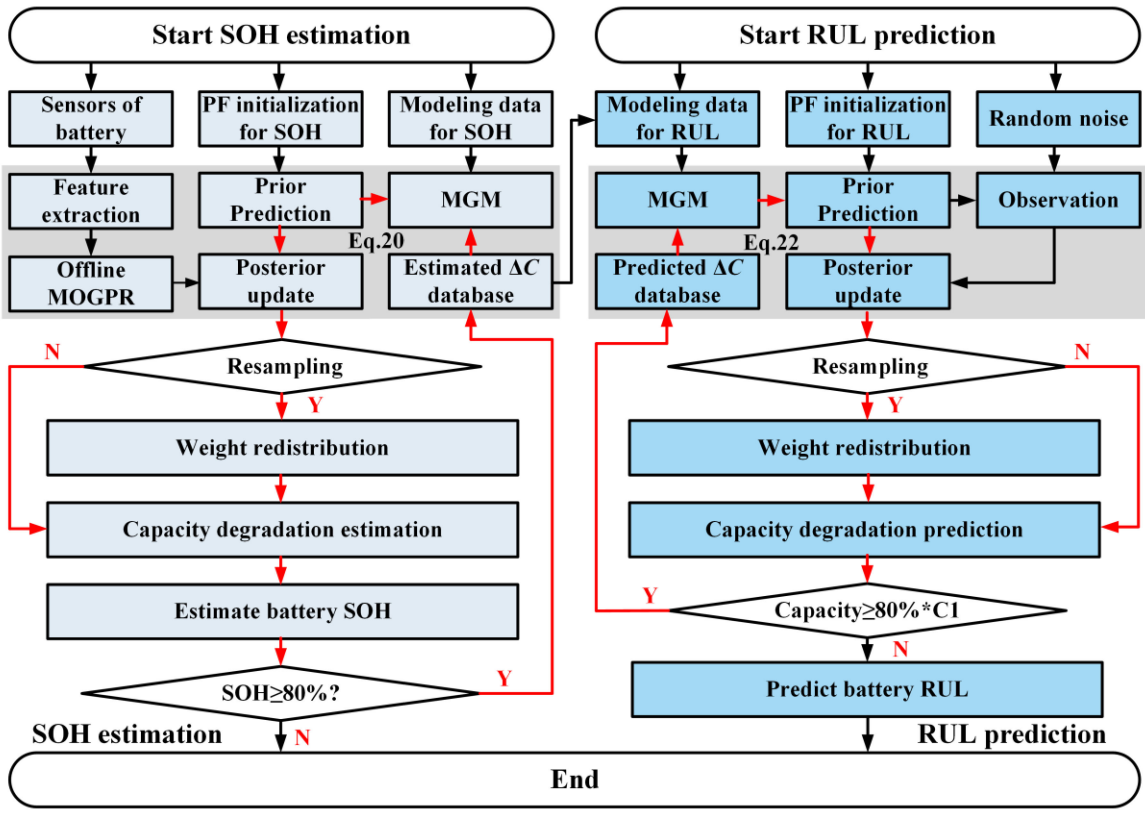

Fig. 7. Flowchart of the proposed method for the SOH estimation and RUL prediction.

C. Proposed Methods

To complete the task of SOH estimation based on the proposed model-data-fusion method, a dynamic and data-driven state-space representation is constructed first

$$\begin{cases} \Delta\hat{C}^{-}_{k+1} = \mathrm{MGM}\left(\Delta\hat{C}^{+}_{k-m}, \cdots, \Delta\hat{C}^{+}_{k}\right) + w_k \\ \begin{bmatrix} \Delta\hat{R}^{k+1}_{0} \\ \Delta\hat{R}^{k+1}_{1} \end{bmatrix} = \mathrm{MOGPR}\left(\Delta\hat{C}^{-}_{k+1},\ T\right) + v_{k+1} \end{cases} \tag{20}$$

where $\Delta\hat{C}^{-}_{k+1}$ represents the MGM-based prior estimation of capacity degradation, $\Delta\hat{R}^{k+1}_{0}$, $\Delta\hat{R}^{k+1}_{1}$ represents the estimated ageing features through MOGPR, and T represents temperature.

With the state-space representation, PF can update $\Delta\hat{C}^{-}_{k+1}$ and obtain the posterior state ($\Delta\hat{C}^{+}_{k+1}$) using the ageing features as inputs. Then, the output ($\Delta\hat{C}^{+}_{k+1}$) is fed back to update the state-space representation [see (20)] again.

Then, the SOH can be calculated by

$$SOH_k = \frac{C_1 - \Delta\hat{C}^{+}_{k}}{C_1} \times 100\%. \tag{21}$$

For RUL mentioned in (1), the essential of RUL prediction is to estimate $Cycle_{\mathrm{total}}$. However, to complete the RUL prediction in EVs, two problems remain to be solved: 1) The battery actual capacity cannot be measured. Thus, to predict battery RUL, the estimated capacity dataset is adopted; 2) Future ageing features cannot be acquired. Herein, we use the prediction and random noise to describe the predicted degradation trajectory of LIBs. Moreover, historic capacities are preserved to avoid violent divergency. Finally, a state-space representation for the RUL prediction is constructed as

$$\begin{cases} \Delta\hat{C}^{-}_{k+1} = \mathrm{MGM}\left(\Delta\hat{C}^{+}_{1}, \cdots, \Delta\hat{C}^{+}_{k}\right) + w_{k+1} \\ \Delta\hat{C}^{+}_{k+1} = \Delta\hat{C}^{-}_{k+1} + v_{k+1}. \end{cases} \tag{22}$$

Based on the state-space representation, the battery capacity degradation ($\Delta\hat{C}^{+}_{k+1}$) is extrapolated through PF. When the predicted capacity degradation reaches the life threshold, RUL is determined.

To sum up, a flowchart of the proposed model-data-fusion method for the battery SOH estimation and RUL prediction is shown in Fig. 7.

As can be seen from Fig. 7, there are a few steps that need to be implemented in sequence to implement the proposed method for SOH estimation and RUL prediction

Step 1: State-space representation construction for SOH estimation.

1) In each modeling, four historic capacity degradation data were used for model initialization [Data Model Initialization (DMI) = 4], the MGM is employed to construct the state equation.
2) The capacity degradation and ageing features of the reference battery are extracted as the offline input and output of MOGPR, respectively, to form the observation equation.
3) Combined MGM-based state equation and MOGPR-based observation equation, a dynamic and data-driven

state-space representation is constructed to describe the battery degradation, as shown in (20).

Step 2: PF for capacity degradation trajectory tracking.

1) The initial capacity degradation and weight distribution are set according to Step 1 of PF.
2) For the validation battery, the next-time prior capacity degradation is predicted by the MGM-based state equation in step (1.1) based on Step 2 of PF.
3) The ageing features and temperature of the validation battery are extracted and imported into the trained MOGPR-based observation equation in step (1.2); then, we can obtain the estimated ageing features.
4) Based on the PF-based framework and step (2.3), the prior capacity degradation is updated using the online ageing features of the validation battery to obtain posterior capacity degradation based on Step 3 of PF.
5) According to the resampling strategy, the weight of the particles is reassigned based on Step 4 of PF. Then, the SOH is calculated according to (21) based on the particle weight shown in Step 5 of PF. Then, returns to Step 1 to update the state-space representation for the SOH estimation through posterior capacity degradation.

Step 3: State-space representation and PF for RUL prediction.

1) When battery estimated SOH is greater than 80% and RUL prediction is started, the capacity degradation dataset is as the modeling data for the RUL prediction.
2) The MGM is employed to form the state equation, and the sum of capacity and random noise is as the observation equation. Thus, a state-space representation for the RUL prediction is constructed in (22).
3) Based on the PF-based framework and the dynamic state-space representation, battery capacity is extrapolated to the failure threshold ($\leq$80% of initial capacity). Then, $cycle_{\mathrm{total}}$ and RUL are predicted from the extrapolation process.

For purposes of comparison, some common techniques in the previous research works for the SOH estimation and RUL prediction are implemented. Herein, with the same defined ageing features (ΔR_0 and ΔR_1), the commonly used and the effective data-driven methods, GPR [46] and SVR [21], are used to estimate SOH, while 6-rd polynomial model [23] and double exponential model [47] are used to predict RUL.

V. Results Verification and Discussion

This section evaluates the performance of the proposed model-data-fusion method for the SOH estimation and RUL prediction using the datasets obtained in Section II. To avoid the single verification mode and improve the data utilization, the ageing features are extracted by randomly selecting one cycle data from three dynamic loading profiles. Besides, the dataset for offline ageing feature-based battery degradation model construction is selected randomly at different temperatures, as shown in Table III. Thus, such a verification mode can adequately assess the performance of the proposed method using the two batteries, respectively.

TABLE III
Battery Number for Data Selection

Temperature	Reference battery	Validation battery
10°C	NO. A	NO. B
25°C	NO. B	NO. A
40°C	NO. A	NO. B

TABLE IV
Numeric Results of the SOH Estimation

Method	Index	10°C	25°C	40°C
Proposed	RMSE/%	0.6596	0.5086	0.7250
	STD/%	0.6650	0.5154	0.7277
GPR	RMSE/%	1.1184	0.6986	1.5893
	STD/%	0.9617	0.7053	1.5578
SVR	RMSE/%	2.5507	0.8456	0.7628
	STD/%	2.5828	0.8537	0.7716

Herein, the particle number is set as 200, and the residual resampling method is as the resampling strategy. In addition, for the simulations of this proposed method, the software and hardware platform configuration information are as follows: Desktop, Intel Core i7-7700K 4.2G CPU, 32G DDR3 RAM, Windows 10, MATLAB R2018a.

A. Verification of the SOH Estimation

For the validation of the proposed SOH estimation method, the two batteries' ageing datasets are applied for simulation at different temperatures, respectively. The capacity degradation is first estimated, then battery SOH is calculated through (21). According to Table III, SOH estimation results using the proposed method at different temperatures are shown in Fig. 8. Besides, the SOH estimation results of the contrast methods at different temperatures are shown in Supplementary Figs. 1 to 6. As illustrated in Fig. 8, battery SOH decreases with ageing, and the proposed model-data-fusion method can track the capacity degradation trajectory effectively at different temperatures. Besides, it does occur the capacity regeneration during the whole life, however, the model-data-fusion method can quickly return to actual degradation trajectory and achieve accurate SOH estimation. Also, 95% CIs of SOH estimation are given, the narrower CI represents a stronger reliability of the SOH estimation. Combining Figs. 2 and 8, although the capacity difference between two battery becomes bigger with ageing, the CIs and errors in the whole life tend to converge and are no more than $\pm$ 2%. Besides, there is no obvious correlation between temperatures and errors. The results imply that the SOH estimation is accurate and robust.

To quantificationally evaluate the performance of different methods for the SOH estimation, the root mean squared error (RMSE) and error standard deviation (STD) are calculated, the results are shown in Table IV. The RMSE is a standard statistical metric to measure the dispersion degree and convergence performance between estimated and real curves of SOH. The STD is employed to measure the overall fluctuation trend of SOH estimation errors.

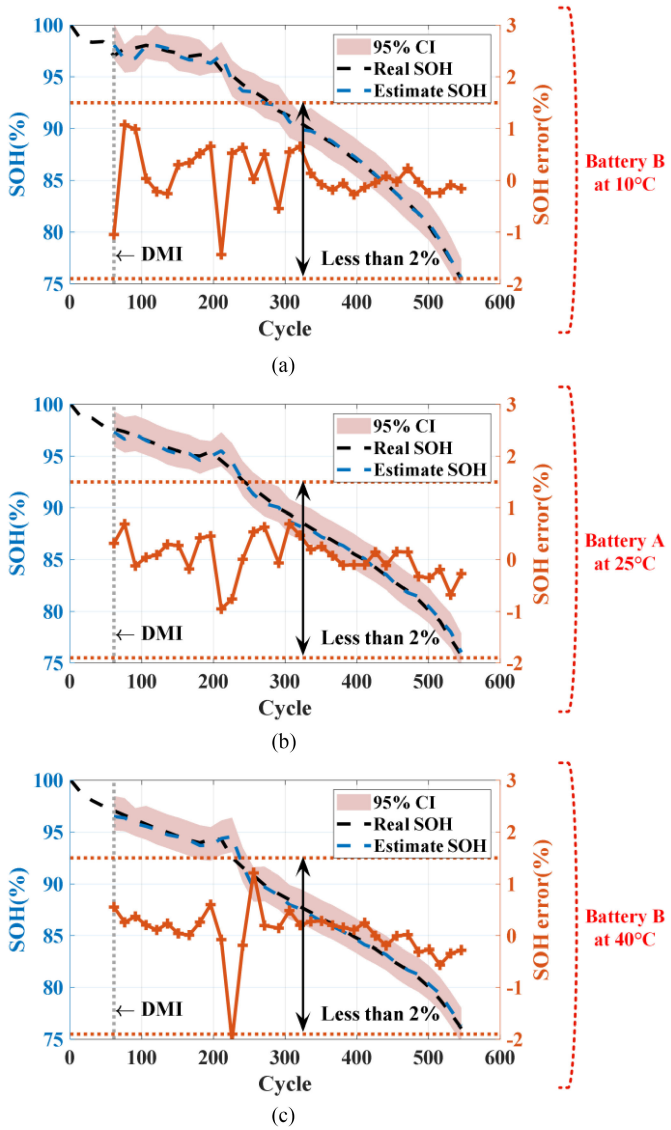

Fig. 8. SOH estimation results for different batteries at different temperatures.

As shown in Table IV, the RMSE and STD of the proposed method for the SOH estimation are maintained about 1% at different temperatures, which are less than GPR and SVR. Therefore, it can be concluded that the model-data-fusion method for the SOH estimation is available and has higher accuracy and stronger robustness than the contrast methods owing to the closed-loop control and dynamic model updating.

B. Verification of the RUL Prediction

Based on an accurate SOH estimation, battery RUL prediction is implemented. In this case, the RUL threshold is set to 80% of initial capacity at different temperatures, then, battery RUL is predicted at 60% and 80% of the whole lifetime, respectively. The graphical results of RUL prediction are shown in Fig. 9, while the results of the 6-rd polynomial model and double exponential model are shown in Supplementary Figs. 7 to 18. Meanwhile, the absolute errors of the three models for the RUL prediction with different starting points are listed in Table V. It is important to point out that the battery goes through about 15 cycles between two adjacent data points (see Table I), the actual RUL is determined by the linear interpolation.

TABLE V
ABSOLUTE ERRORS OF THE RUL PREDICTION

Model	Starting	10°C	25°C	40°C
Proposed	60%	31	40	54
	80%	3	2	2
6-rd polynomial model	60%	114	28	78
	80%	54	61	46
Double exponential model	60%	93	123	108
	80%	12	3	3

As illustrated in Fig. 9, using the SOH estimates as the modeling data to extrapolate the battery capacity degradation, the predicted capacity is slightly smaller than the actual capacity due to the smaller capacity estimates. Besides, the capacity trajectories produced through the model-data-fusion method are approximately consistent with the actual capacity trajectories, and especially accord with the characters of actual capacity trajectories when more capacity data are obtained. In addition, the probability density function (PDF) of the capacity estimates reflects the uncertainty of the RUL prediction. The entire PDF can be equivalently represented using its mean (or center) and variance (or width), and the mean of PDF distribution represents the accuracy of the RUL prediction while the variance represents the uncertainty of RUL. As the predicted starting point moves backward (from 60% to 80% of the lifetime), the distributions of PDF on the *X*-axis become narrower and the peaks become higher, which indicates that the uncertainty of the results of the RUL prediction becomes smaller. For instance, at 10 °C, when the RUL prediction is started at 60% of the lifetime, the prediction error is 31 cycle, while 80% of the lifetime is as the prediction starting point, the prediction error is significantly reduced to three cycles. That is, the accuracy of the RUL gradually increases, and the uncertainty of RUL gradually reduces when more SOH estimates are used for modeling. Similar results can be attained at the other two temperatures for the proposed model-data-fusion method. Compared with the 6-rd polynomial model and double exponential model, the proposed method has smaller absolute errors at different starting prediction points and temperatures (see Table V). In addition, there is not a divergent phenomenon for the proposed model-data-fusion method to predict capacity degradation comparing with the other two models.

C. Time Analysis of the SOH Estimation and RUL Prediction

To further evaluate the computation complexity of the proposed methods, the time consumptions for SOH and RUL prediction are counted. Meanwhile, the time for the methods of comparison is counted as illustrated in Fig. 10. For SOH estimation, the proposed method requires about 1 to 1.2 s to complete all the calculations. By contrast, GPR and SVR have

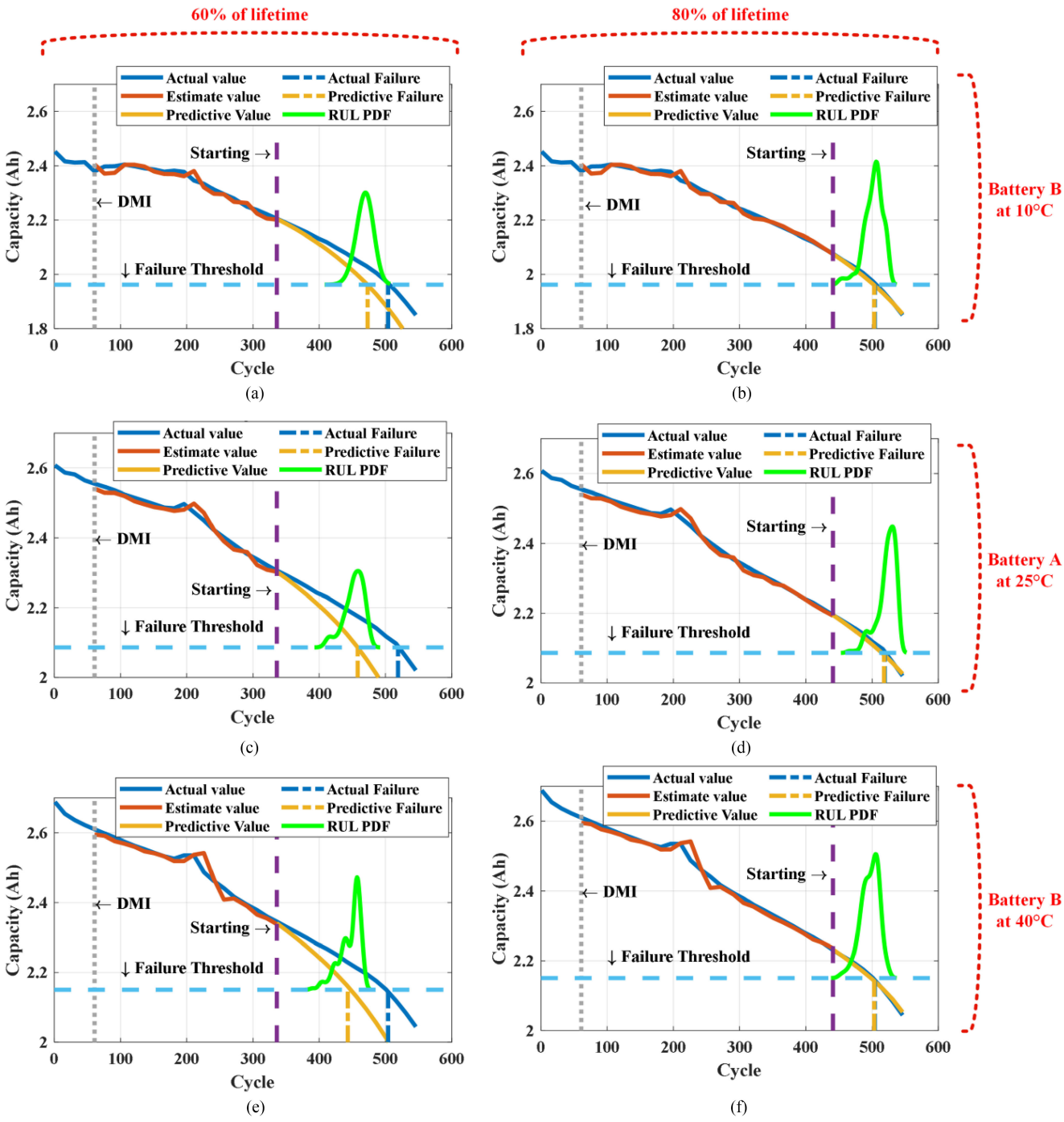

Fig. 9. RUL prediction results of different batteries at different temperatures.

faster computation speed [see Fig. 10(a)]. The main reason is that the proposed method needs to forecast and update capacity degradation except for offline training. In general, the proposed method provides higher estimation accuracy with longer time consumptions. For the RUL prediction, the three ageing models adopt the same prediction framework using the SOH datasets. Therefore, different ways and data for modeling lead to different time consumptions. As shown in Fig. 10(b) and (c), the three models have similar modeling time in milliseconds level. Besides, the RUL prediction using 80% of the lifetime costs more time than using 60% of the lifetime due to more modeling data for prediction.

Summing up the above results, the proposed methods can achieve accurate SOH estimation. Based on the estimated SOH, RUL is predicated at different in starting point with high estimation accuracy. In consideration of the computational accuracy and time consumption, the proposed methods have better performance for the SOH estimation and RUL prediction than some previous works. Therefore, the model-data-fusion method can accurate SOH and RUL and valuable pieces of information

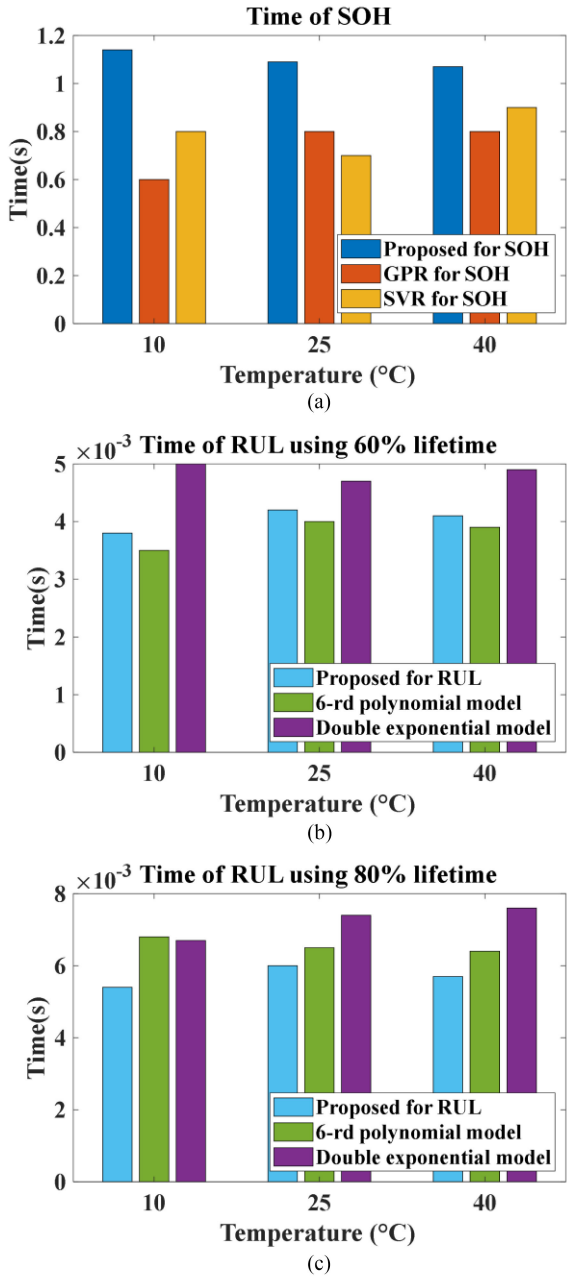

Fig. 10. Time analysis on SOH and RUL.

necessary for maintenance decision for the degraded batteries in EVs.

For the battery management algorithms on the SOH estimation and RUL prediction in EVs, it is significant to embed the key algorithms into an on-board BMS. Herein, the proposed method for SOH estimation consists of the MGM-based state equation, MOGPR-based observation equation, and PF. Only the observation equation required offline training. Then, by combining the offline MOGPR battery degradation model, MGM, and PF, the framework for the SOH estimation can be also embedded into a BMS. For the method for RUL, the modeling data are from the SOH estimation, and the whole framework can be also implemented online.

VI. Conclusion

In this article, a model-data-fusion method for the SOH estimation and RUL prediction is proposed. The major contributions are summarized as follows. First, based on existing work, two resistance-based ageing features from battery Thevenin model are expanded to different temperatures. The underlying relationship between capacity degradation and ageing features, the coupling relationship between two ageing features are evaluated by the correlation analysis. Second, the MGM is employed to construct a state equation for time update. The MOGPR is used to construct an observation equation for observation update based on the measurable ageing features. Then, a dynamic and data-driven state-space representation is proposed to describe the battery capacity degradation. Third, based on the state-space representation, PF is introduced to build a model-data-fusion framework for the SOH estimation and RUL prediction. Fourth, the battery under various dynamic profiles and temperatures are used to verify the proposed method. Owing to the closed-loop control and dynamic model updating, the proposed method is shown to be accurate and robust based on the results of SOH estimation and RUL prediction.

To summarize, the proposed method has significant advantages of high accuracy, strong robustness, and probabilistic output. Besides, the model-data-fusion method has the potential to be suitable for other batteries with different cathode materials when the degradation model is retrained according to the objective batteries. In the future, we will try to optimize the current degradation model to provide a more accurate and faster SOH estimation and the RUL perdition using less computation demanding. Moreover, intelligent resampling technology will be paid more attention to improve the performance of PF. Also, the hardware in the loop for real-time simulation in BMS is being developed to verify the practicability of the method.

Acknowledgment

The authors would like to thank and pay high tribute to Prof.Daming Zhou at Northwestern Polytechnical University, for his instructive suggestions on the revisions of the work in this article.

References

[1] C. Pastor-Fernández, T. F. Yu, W. D. Widanage, and J. Marco, "Critical review of non-invasive diagnosis techniques for quantification of degradation modes in lithium-ion batteries," *Renewable Sustain. Energy Rev.*, vol. 109, pp. 138–159, 2019.

[2] X. Hu, F. Feng, K. Liu, L. Zhang, J. Xie, and B. Liu, "State estimation for advanced battery management: Key challenges and future trends," *Renewable Sustain. Energy Rev.*, vol. 114, 2019, Art. no. 109334.

[3] J. Wei, G. Dong, and Z. Chen, "Remaining useful life prediction and state of health diagnosis for lithium-ion batteries using particle filter and support vector regression," *IEEE Trans. Ind. Electron.*, vol. 65, no. 7, pp. 5634–5643, Jul. 2018.

[4] M. S. H. Lipu *et al.*, "A review of state of health and remaining useful life estimation methods for lithium-ion battery in electric vehicles: Challenges and recommendations," *J. Cleaner Prod.*, vol. 205, pp. 115–133, 2018.

[5] R. Xiong, L. Li, and J. Tian, "Towards a smarter battery management system: A critical review on battery state of health monitoring methods," *J. Power Sources*, vol. 405, pp. 18–29, 2018.

[6] X. Li, Z. Wang, L. Zhang, C. Zou, and D. D. Dorrell, "State-of-health estimation for Li-ion batteries by combing the incremental capacity analysis method with grey relational analysis," *J. Power Sources*, vol. 410–411, pp. 106–114, 2019.

[7] M. Berecibar, M. Garmendia, I. Gandiaga, J. Crego, and I. Villarreal, "State of health estimation algorithm of $LiFePO_4$ battery packs based on differential voltage curves for battery management system application," *Energy*, vol. 103, pp. 784–796, 2016.

[8] X. Hu, J. Jiang, D. Cao, and B. Egardt, "Battery health prognosis for electric vehicles using sample entropy and sparse bayesian predictive modeling," *IEEE Trans. Ind. Electron.*, vol. 63, no. 4, pp. 2645–2656, Apr. 2016.

[9] R. Xiong, *Battery Management Algorithm for Electric Vehicles*. Berlin, Germany: Springer, 2020.

[10] R. Xiong and W. Shen, *Advanced Battery Management Technologies for Electric Vehicles*. Hoboken, NJ, USA: Wiley, 2018.

[11] L. Zheng, L. Zhang, J. Zhu, G. Wang, and J. Jiang, "Co-estimation of state-of-charge, capacity and resistance for lithium-ion batteries based on a high-fidelity electrochemical model," *Appl. Energy*, vol. 180, pp. 424–434, 2016.

[12] C. Lin, J. Xing, and A. Tang, "Lithium-ion battery state of charge/state of health estimation using SMO for EVs," *Energy Procedia*, vol. 105, pp. 4383–4388, 2017.

[13] C. Lyu *et al.*, "In situ monitoring of lithium-ion battery degradation using an electrochemical model," *Appl. Energy*, vol. 250, pp. 685–696, 2019.

[14] J. Li, K. Adewuyi, N. Lotfi, R. G. Landers, and J. Park, "A single particle model with chemical/mechanical degradation physics for lithium ion battery state of health (SOH) estimation," *Appl. Energy*, vol. 212, pp. 1178–1190, 2018.

[15] Y. Zou, X. Hu, H. Ma, and S. E. Li, "Combined state of charge and state of health estimation over lithium-ion battery cell cycle lifespan for electric vehicles," *J. Power Sources*, vol. 273, pp. 793–803, 2015.

[16] H. H. Afshari, M. Attari, R. Ahmed, A. Delbari, S. Habibi, and T. Shoa, "Reliable state of charge and state of health estimation using the smooth variable structure filter," *Control Eng. Pract.*, vol. 77, pp. 1–14, 2018.

[17] S. Schwunk, N. Armbruster, S. Straub, J. Kehl, and M. Vetter, "Particle filter for state of charge and state of health estimation for lithium–iron phosphate batteries," *J. Power Sources*, vol. 239, pp. 705–710, 2013.

[18] E. Shi, F. Xia, D. Peng, L. Li, X. Wang, and B. Yu, "State-of-health estimation for lithium battery in electric vehicles based on improved unscented particle filter," *J. Renewable Sustain. Energy*, vol. 11, 2019, Art. no. 024101.

[19] C. Piao, Z. Li, S. Lu, Z. Jin, and C. Cho, "Analysis of real-time estimation method based on hidden Markov models for battery system states of health," *J. Power Electron.*, vol. 16, pp. 217–226, 2016.

[20] G. You, S. Park, and D. Oh, "Diagnosis of electric vehicle batteries using recurrent neural networks," *IEEE Trans. Ind. Electron.*, vol. 64, no. 6, pp. 4885–4893, Jun. 2017.

[21] J. Meng, L. Cai, G. Luo, D. Stroe, and R. Teodorescu, "Lithium-ion battery state of health estimation with short-term current pulse test and support vector machine," *Microelectron. Rel.*, vol. 88–90, pp. 1216–1220, 2018.

[22] P. Guo, Z. Cheng, and L. Yang, "A data-driven remaining capacity estimation approach for lithium-ion batteries based on charging health feature extraction," *J. Power Sources*, vol. 412, pp. 442–450, 2019.

[23] Y. Zhang, R. Xiong, H. He, and M. G. Pecht, "Lithium-ion battery remaining useful life prediction with box–cox transformation and Monte Carlo simulation," *IEEE Trans. Ind. Electron.*, vol. 66, no. 2, pp. 1585–1597, Feb. 2019.

[24] C. Liu, Y. Wang, and Z. Chen, "Degradation model and cycle life prediction for lithium-ion battery used in hybrid energy storage system," *Energy*, vol. 166, pp. 796–806, 2019.

[25] W. He, N. Williard, M. Osterman, and M. Pecht, "Prognostics of lithium-ion batteries based on Dempster–Shafer theory and the Bayesian Monte Carlo method," *J. Power Sources*, vol. 196, pp. 10314–10321, 2011.

[26] X. Zhang, Q. Miao, and Z. Liu, "Remaining useful life prediction of lithium-ion battery using an improved UPF method based on MCMC," *Microelectron. Rel.*, vol. 75, pp. 288–295, 2017.

[27] E. Walker, S. Rayman, and R. E. White, "Comparison of a particle filter and other state estimation methods for prognostics of lithium-ion batteries," *J. Power Sources*, vol. 287, pp. 1–12, 2015.

[28] P. L. T. Duong and N. Raghavan, "Heuristic Kalman optimized particle filter for remaining useful life prediction of lithium-ion battery," *Microelectron. Rel.*, vol. 81, pp. 232–243, 2018.

[29] B. Saha, K. Goebel, S. Poll, and J. Christophersen, "Prognostics methods for battery health monitoring using a Bayesian framework," *IEEE Trans. Instrum. Meas.*, vol. 58, no. 2, pp. 291–296, Feb. 2009.

[30] Y. Zhou, M. Huang, Y. Chen, and Y. Tao, "A novel health indicator for on-line lithium-ion batteries remaining useful life prediction," *J. Power Sources*, vol. 321, pp. 1–10, 2016.

[31] T. Parthiban, R. Ravi, and N. Kalaiselvi, "Exploration of artificial neural network [ANN] to predict the electrochemical characteristics of lithium-ion cells," *Electrochimica Acta*, vol. 53, pp. 1877–1882, 2007.

[32] D. Liu, J. Zhou, D. Pan, Y. Peng, and X. Peng, "Lithium-ion battery remaining useful life estimation with an optimized relevance vector machine algorithm with incremental learning," *Measurement*, vol. 63, pp. 143–151, 2015.

[33] P. Khumprom and N. Yodo, "A data-driven predictive prognostic model for lithium-ion batteries based on a deep learning algorithm," *Energies*, vol. 12, 2019, Art. no. 660.

[34] X. Li, L. Zhang, Z. Wang, and P. Dong, "Remaining useful life prediction for lithium-ion batteries based on a hybrid model combining the long short-term memory and Elman neural networks," *J. Energy Storage*, vol. 21, pp. 510–518, 2019.

[35] H. Pan, Z. Lü, H. Wang, H. Wei, and L. Chen, "Novel battery state-of-health online estimation method using multiple health indicators and an extreme learning machine," *Energy*, vol. 160, pp. 466–477, 2018.

[36] Z. Lyu and R. Gao, "A model-based and data-driven joint method for state-of-health estimation of lithium-ion battery in electric vehicles," *Int. J. Energy Res.*, vol. 43, pp. 7956–7969, 2019.

[37] Z. Lyu and R. Gao, "Li-ion battery state of health estimation through Gaussian process regression with Thevenin model," *Int. J. Energy Res.*, vol. 44, pp. 10262–10281, 2020.

[38] X. Hu, S. Li, and H. Peng, "A comparative study of equivalent circuit models for Li-ion batteries," *J. Power Sources*, vol. 198, pp. 359–367, 2012.

[39] J. Bi, T. Zhang, H. Yu, and Y. Kang, "State-of-health estimation of lithium-ion battery packs in electric vehicles based on genetic resampling particle filter," *Appl. Energy*, vol. 182, pp. 558–568, 2016.

[40] R. Xiong, H. He, F. Sun, and K. Zhao, "Evaluation on state of charge estimation of batteries with adaptive extended Kalman filter by experiment approach," *IEEE Trans. Veh. Technol.*, vol. 62, no. 1, pp. 108–117, Jan. 2013.

[41] S. Sankararaman and K. Goebel, "Why is the remaining useful life prediction uncertain," *Annual Conference of the Prognostics and Health Management Society*, 2013.

[42] M. Jouin, R. Gouriveau, D. Hissel, M. Péra, and N. Zerhouni, "Particle filter-based prognostics: Review, discussion and perspectives," *Mech. Syst. Signal Process.*, vol. 72/73, pp. 2–31, 2016.

[43] L. Chen *et al.*, "Remaining useful life prediction of battery using a novel indicator and framework with fractional grey model and unscented particle filter," *IEEE Trans. Power Electron.*, vol. 35, no. 6, pp. 5850–5859, Jun. 2020.

[44] H. Liu, J. Cai, and Y.-S. Ong, "Remarks on multi-output Gaussian process regression," *Knowl. Syst.*, vol. 144, pp. 102–121, 2018.

[45] R. R. Richardson, C. R. Birkl, M. A. Osborne, and D. A. Howey, "Gaussian process regression for *in situ* capacity estimation of lithium-ion batteries," *IEEE Trans. Ind. Inform.*, vol. 15, no. 1, pp. 127–138, Jan. 2019.

[46] X. Li, C. Yuan, X. Li, and Z. Wang, "State of health estimation for Li-ion battery using incremental capacity analysis and Gaussian process regression," *Energy*, vol. 190, 2020, Art. no. 116467.

[47] H. Zhang, Q. Miao, X. Zhang, and Z. Liu, "An improved unscented particle filter approach for lithium-ion battery remaining useful life prediction," *Microelectron. Rel.*, vol. 81, pp. 288–298, 2018.